APPLICATIONS PAPER

Multitemporal Landsat Image Based Water Quality Analyses of Danjiangkou Reservoir

Yinuo Zhang, Xin Huang, and Dun Zhu

Abstract

Danjiangkou Reservoir (DJKR) is one of the largest artificial freshwater lakes in Asia and a water source of the South: the North Water Transfer Project. However, few studies have analyzed the spatio-temporal water quality distribution or investigated the causative factors of the long-term water quality variation of DJKR. In this study, we used multi-temporal Landsat images combined with the multiple linear stepwise regression (MLSR) method to retrieve long-term distributions of the main water quality parameters in DJKR, i.e., total nitrogen (TN), total phosphorus (TP), permanganate index (COD_{Mn}), and five-day biochemical oxygen demand (BOD_5). Results indicated the heavily polluted regions and an alarming water quality deterioration trend between May 2006 and May 2014. A combination of land use/land cover (LULC) maps and socio-economic data was considered to investigate the causative factors of the water quality distribution, as well as the deterioration. This study could provide a valuable reference for the decision-making for water quality conservation in DJKR.

Introduction

Freshwater is indispensable for our lives and daily activities. However, China comprises 22 percent of the World's population but contains only 7 percent of the total surface freshwater on Earth (Li *et al.*, 2009). Influenced by the monsoon climate and the mismanagement of water and soil resources, the water distribution in China is highly heterogeneous. In other words, less than 20 percent of the freshwater distributes in North China, which accounts for 63.5 percent of China's land area. As a consequence, the North China Plain contains 0.35 billion people, yet has per capita water resources of only 456 m^3, which is less than one-quarter of China's average. Therefore, the South-North Water Transfer (SNWT) Project was officially launched in 2002 to solve this problem. The project has been one of the largest strategic projects in China since 1949 and has received global attention. This formidable and arduous project has three routes: the eastern and middle routes aim to channel water to North China, and the western route diverts water to Northwest China. Danjiangkou Reservoir (DJKR), located on the Han River, which is the longest tributary of the Yangtze River, is the one of the largest artificial freshwater lakes in Asia, with a surface area of ~1000 km^2 and a volume of ~29 billion m^3. It was therefore chosen to be the water source of the middle route of the SNWT Project, which aims to supply up to 13.8 billion m^3 of freshwater annually to the North China Plain, including two municipalities (Beijing and Tianjin), and more than 130 other cities, for domestic, industrial, and agricultural use (Li and Zhang, 2005).

Yinuo Zhang and Xin Huang are with the State Key Laboratory of Information Engineering in Surveying, Mapping and Remote Sensing, Wuhan University, Luoyu Road No.129, Wuhan, Hubei Province, P.R.China (huang_whu@163.com).

Wei Yin and Dun Zhu are with the Yangtze River Water Resources Protection Science Institute, Qintai Avenue No. 515, Wuhan, Hubei Province, P.R.China.

In addition, DJKR is one of the water sources of "NongFu Spring", which has been one of the most popular drinking water brands of China since 1996 and produces over 0.6 million tons of natural drinking water annually. The water quality of DJKR directly affects the drinking water security of hundreds of millions of Chinese people and the implementation of the largest-ever water transfer project. Therefore, periodic and efficient water quality monitoring in DJKR is urgently needed.

Traditional *in-situ* measurements are able to provide details of the optical properties of water, and they provide accurate data at fixed sample sites in DJKR. Nevertheless, this approach is not only costly and time-consuming, but also restricted by natural conditions, e.g. weather and terrain (Guan *et al.*, 2011). Moreover, traditional *in-situ* measurements cannot provide the spatio-temporal distributions of the water quality parameters (Chen *et al.*, 2015), and hence limit the comprehensiveness of the water quality monitoring. With the advent of satellite images, they have been widely used for inland water quality monitoring due to their extraordinary ability of providing a synoptic view of water properties over a large-scale spatial area (Chen and Quan, 2012). Landsat imagery are generally applied in this situation, as they feature a global coverage, the longest record of Earth observation, free access, high-resolution, as well as multispectral data (Loveland and Dwyer, 2012). The instructive application of multi-temporal Landsat images in previous studies has confirmed their potential in large-scale water quality monitoring. For instance, Lathrop and Richard (1992), Kloiber *et al.* (2002), Ritchie (2003), and McCullough *et al.* (2012) used multi-temporal Landsat images to perform long-term analyses of water clarity. Pastorguzman *et al.* (2015) and Tebbs *et al.* (2013) applied Landsat ETM+ bands to estimate chlorophyll-a (*Chl-a*) concentration and successfully related the results to the local algal blooms. Brezonik *et al.* (2005) made a characterization of the optical properties between *Chl-a* and colored dissolved organic matter (CDOM) using empirical models. Recently, Lobo *et al.* (2015) proposed a non-linear empirical regression model to estimate TSS in the Tapajós River Basin, and then combined it with the impact of gold mining activities.

However, little attention has been paid to the application of satellite images in DJKR. In addition, the existing pertinent studies have provided an insight mainly into *Chl-a*, CDOM, and water clarity, but they have neglected the many other important water quality parameters, such as total nitrogen (TN), total phosphorus (TP), permanganate index (COD_{Mn}), and five-day biochemical oxygen demand (BOD_5), which are also closely related to anthropogenic activities and contribute to the eutrophication of the lakes and reservoirs.

The purpose of this study was to apply multi-temporal and multi-sensor Landsat images (TM, ETM+, and OLI) of DJKR from

Photogrammetric Engineering & Remote Sensing
Vol. 83, No. 9, September 2017, pp. 33–xxx.
0099-1112/17/33–xxx

doi: 10.14358/PERS.83.9.xxx

2006 to 2014, as well as routine *in-situ* datasets, to retrieve a synoptic view of the distribution of COD_{Mn}, BOD_5, TP, and TN, which are the main parameters of the routine water quality monitoring in DJKR. Furthermore, we provided insights into the influence of the tributaries on the spatio-temporal distribution and variation of the water quality parameters, considering that few of the existing studies took into account the impacts of the tributaries on the water quality conditions. The multiple linear stepwise regression (MLSR) method was employed to develop reliable algorithms to extract the aforementioned water quality parameters. We then discussed the seasonal distribution and annual water quality variability. The water quality results were subsequently used to examine possible pollution sources in both the reservoir and tributaries. The land use/land cover (LULC) maps and statistical data series were also incorporated into a synthetic discussion on the causative factors of the water quality deterioration. The results of this study will provide an essential and timely reference for the water quality improvement in the DJKR catchment area.

Materials

Study Area

Danjiangkou Reservoir (DJKR, 32°36′ to 33°48′N, 110°59′ to 111°49′E) is located on the upstream of the Han River at the junction of Hubei and Henan provinces, Central China (Figure 1). It is recognized as one of the largest artificial freshwater lakes in Asia, with a surface area of ~1000 km^2 and a volume of ~29 billion m^3 (after the dam was raised in 2005). Therefore, DJKR is known as the "Water Capital" and was assigned to be the source of the middle route of the SNWT Project. In accordance with the distribution of the two main tributaries, the Han River and the Dan River, DJKR is ordinarily divided into two parts: Han Reservoir, which is connected with the Han River in Hubei province; and the Dan Reservoir connected with the Dan River in Henan province. The area of the DJKR watershed is 95,200 km^2, and the average annual inflow is 39.48 billion m^3, 90 percent of which comes from the Han River and the rest from the Dan River. The elevations within the whole watershed, which is surrounded by mountain ranges, e.g., the Qin Mountains, range from 150 m to 3,612 m. The average annual precipitation is over 850 mm, with a clear seasonal variation, and about 80 percent of the annual precipitation occurs during May to October due to the typical subtropical monsoon climate.

Characterized by its diverse biocoenoses and land structures, the DJKR catchment area is a complex eco-environment. Specifically, in terms of the Chinese soil classification system (Li *et al.*, 2009), the soil types of this area consist of brown soil, yellow-brown soil, yellow-cinnamon soil, paddy soil, calcareous soil, chao soil, and purple soil. The purple soil, in particular, is believed to be responsible for most of the sediment in the Yangtze River, as well as its tributaries, including the Han River. Forest vegetation covers approximately 35 percent of the catchment area (Gu *et al.*, 2008), and large areas of farmland are distributed adjacent to the reservoir, especially the eastern and northern parts of Dan Reservoir in Henan Province. A large proportion of the 13 million residents in the upper Han River are peasants (Zhang *et al.*, 2009). In addition, there are four state-level poverty-stricken counties (i.e., Yunyang, Yunxi, Xichuan, and Danjiangkou) and one prefecture-level city, Shiyan, which is well known for its automobile industry, located along the tributaries. Yunyang, Yunxi, and Xichuan counties are subordinate to Shiyan. As a result, intensive agricultural and industrial activities are found along the rivers and streams.

Satellite Data Selection

Landsat, which was first launched in 1972 and has since experienced seven successful missions, has established an unprecedented 43-year record of observations of the global land surface, land conditions, and dynamics (Loveland and Dwyer, 2012). In addition, it has attracted a large number of researchers due to its free access, relatively high spatial resolution, and fine spectral trajectories. In this study, 22 Landsat images (path 125, row 37) with less than 10 percent cloud cover and high signal-to-noise ratio (SNR) were carefully selected from three different sensors (i.e. TM, ETM+, and OLI) in the period between 2006 and 2014. These images were used to retrieve the spatio-temporal distributions of a set of water quality parameters and to investigate the causative factors of water quality in DJKR. As mentioned earlier, about 80 percent of the annual precipitation occurs during May to October in the study area. We therefore refer to May to October as the "wet season", while the rest of the year is referred to as the "dry season". Images in both the wet and dry seasons were applied to examine the seasonal distributions of the water quality parameters, considering the significant distinctions between the hydrologic conditions in different seasons (Feng *et al.* 2016). Nine images of 2013, including five in the wet season and four in the dry season, were deliberately selected for model development in view of their relatively intensive sample sites. The remaining images were used for validation in the experiments. All of the images were Level 1T (L1T) data provided by the United States Geological Survey (USGS 2014). The chosen images are listed in Table 1. The time window, which was defined as the time difference between the date of the image acquisition versus the in-situ data, was set to ±4 days in terms of Bonansea *et al.* (2015) and Lamaro *et al.* (2013).

Table 1. Time Series Landsat Images Used in This Study

Season	Image acquisition date	Sensor	Time window (days)	Season	Image acquisition date	Sensor	Time window (days)
	05-23-2006	TM	−3		11-07-2006	ETM+	−1
	09-15-2007	TM	+4		11-28-2008	ETM+	−4
	09-01-2008	TM	−2		04-08-2010	ETM+	0
	05-07-2009	ETM+	+2		12-04-2010	ETM+	−4
	05-02-2010	TM	−1		01-26-2013	ETM+	−2
	07-08-2011	TM	+3		11-18-2013*	OLI	0
Wet season	09-04-2012	ETM+	+1	Dry season	12-04-2013*	OLI	0
	05-02-2013*	ETM+	0		01-21-2014*	OLI	−1
	06-11-2013*	OLI	+4		03-26-2014*	OLI	−1
	08-06-2013*	ETM+	+1				
	08-14-2013*	OLI	−3				
	09-15-2013*	OLI	−2				
	05-05-2014	ETM+	0				

* Images chosen for model development.

Field Data

It is worth noting that COD_{Mn}, BOD_5, TP, and TN are all routine water quality monitoring parameters of DJKR and their values were all collected at a total of 20 monitoring stations set up by local hydrology departments, with four sampling stations in the reservoir and 16 in the tributaries (Figure 1). Specifically, these four water quality parameters were collected monthly from 2005 to 2013 at the four sampling stations in the reservoir, while the samples in the tributaries were collected semimonthly from 2012 to 2014. Water samples were acquired automatically by the water collecting system at 0.5to 1.0m depth. COD_{Mn}, BOD_5, TP, and TN were all extracted by standard automatic on-line permanganate index analyzer and the analytical techniques for these indices can be found in the Chinese water quality analytical standards, such as Determination of 34 Elements (Pb, Cd, V, P, etc.) (SL 394.1-2007), which has been explained in Xin *et al.* (2015).

To better understand water quality conditions, surface water quality is classified into five grades (Grades I to V) in China according to the Environmental Quality Standards for Surface Water (GB 3838-2002) (*http://www.zhb.gov.cn/*), where a higher grade indicates worse water conditions. Serving as the water source of the SNWT Project, the water quality of DJKR is demanded to be strictly controlled below Grade II, which requires the concentration of COD_{Mn}, BOD_5, TP, and TN to be limited to 4.0 mg/L, 3.0 mg/L, 0.025 mg/L and 0.5 mg/L, respectively.

The 1:100 000 LULC maps of 2005, 2010, and 2015 were mainly generated from the Landsat TM/ETM images with a spatial resolution of 30 m. This dataset was provided by the Data Center for Resources and Environmental Sciences, the Chinese Academy of Sciences (RESDC) (*http://www.resdc.cn/*). The annual wastewater discharge was provided by the Hubei Provincial Department of Water Resources (*http://www.hubeiwater.gov.cn/*), and the annual amounts of chemical fertilizer applied were obtained from the Hubei Statistics Bureau (*http://www.stats-hb.gov.cn/*). These statistical data were used to analyze the water quality variation in the DJKR area.

Methods

Image Preprocessing

The L1T Landsat data provided by the USGS have been geometrically corrected. The geographic coordinates of the 20 sampling stations identified by GPS were used as references for the verification. The results showed that all of the images were geo-referenced with a precision of less than 0.5 pixel. To mask out the haze and cloud cover, we applied a visible/thermal infrared band combination detection method (TM/ETM+ bands 1, 6, 6(RGB) or OLI bands 2, 7, 7(RGB)) (Sriwongsitanon *et al.*, 2011). The digital number (DN) values sensed remotely were converted to the top-of-atmosphere (TOA) radiance values, followed by atmospheric correction based on the Fast Line-of-sight Atmospheric Analysis of Spectral Hypercubes (FLAASH) module embedded in ENVI 5.1. More details of the FLAASH algorithm can be found in Cooley *et al.* (2002), and the main parameters used in the FLAASH module in this study can be found in the metadata in terms of Han *et al.* (2015).

Due to the adjustments of the specific bands of OLI instrument, the spectral response of the OLI bands could be distinct from the corresponding bands of TM/ETM+. Flood (2014) indicated that the TM/ETM+ reflectance could be linearly estimated from the corresponding OLI reflectance based on invariant features, and vice versa. Without losing generality, pseudo-invariant features (PIFs), which were generally acceptable in satellite image normalization, were considered here for the normalization of the between-sensor change. PIFs commonly refer to bright targets (e.g., sand, bare land, concrete construction) and dark targets (e.g., dark dense forests and water bodies) (Du *et al.*, 2002; Lobo *et al.*, 2015). The selection of reliable reference images is a prerequisite for normalization. Considering that OLI bands were better designed for reducing atmospheric effects on spectral response, we chose the radiometrically corrected to a Landsat 8-OLI image acquired on 11 June 2013, as the reference image for the wet seasons, and the radiometrically corrected Landsat 8-OLI image acquired on 18 November 2013, as the reference image for the dry seasons. The bare land, concrete construction, and dense forests were used as the PIFs in this study. The dense forests were identified if the middle-infrared (MIR) band reflectance ρ_{MIR} was greater than or equal to 0.05 and the NDVI was greater than 0.1 according to Song *et al.* (2001). About 90 PIFs were manually selected for each image, and they were all

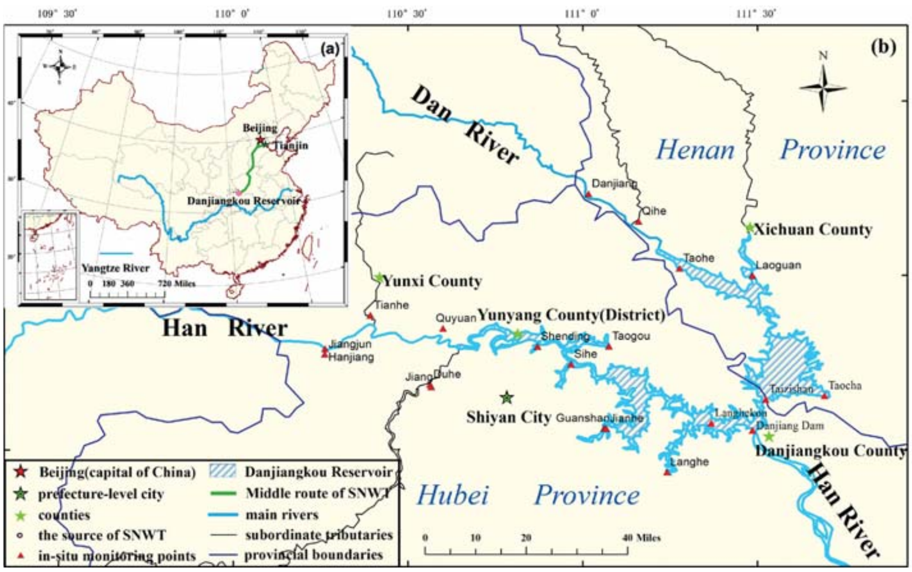

Figure 1. Study area: (a) Overview of the middle route of the SNWT Project, and (b) Location of the Danjiangkou Reservoir catchment area, the sampling stations, and the main rivers and cities.

Table 2. Comparison of the mean pearson correlation coefficients (p <0.05) of the in-situ datasets versus the reflectance values of the OLI bands.

Data	Dry season				Wet season			
	COD_{Mn}	BOD_5	TP	TN	COD_{Mn}	BOD_5	TP	TN
Original	0.55	0.50	0.49	0.53	0.52	0.74	0.60	0.61
Log-transformed	0.51	0.48	0.49	0.49	0.47	0.61	0.47	0.59

evenly distributed close to the DJKR catchment area. Normalization of these images was then accomplished based on ordinary least squares (OLS) regression in terms of Lo and Yang (2000) and Canty *et al*. (2004). The PIFs were reselected until the correlation coefficients of each model reached 0.95 (p <0.05).

Model Development

The modified normalized difference water index (MNDWI) algorithm proposed by Xu (2006) was adopted to extract the boundaries of DJKR and the tributaries. The thresholds were manually adjusted in order to guarantee the accuracy of the footprints of the water areas in the multitemporal Landsat images.

The MSLR method has been widely used to develop empirical water quality models due to its superiority in optimal variable selection (Çamdevýren *et al*., 2005; Sriwongsitanon *et al*., 2011). The Landsat image pixels corresponding to the *in-situ* sample stations were first extracted from the specified images in the dry season and the wet season in 2013 (Table 1), and the mixed pixels were excluded from the water delineation, since some of the sample locations were too close to the land (less than 30 m), especially in the small tributaries. The outliers were then eliminated to optimize the models in terms of Selst and Jolicoeur (1994). Therefore, the final data points used for the regression analyses were 31 in the wet season and 26 in the dry season.

The Kolmogorov-Smirnov (K-S) test indicated that the original and log-transformed COD_{Mn}, BOD_5, and TP, as well as the TN values in both seasons, were all normally distributed. Meanwhile, the original *in-situ* datasets were obviously more Pearson-correlated with the reflectance values of the Landsat OLI bands (Table 2). Consequently, the original COD_{Mn}, BOD_5, TP, and TN values were set as the dependent variables. As Oki (2010) explained, band ratios can effectively reduce the influence of backscattering. Seven bands (OLI bands 1 to 7) and their mutual ratios were therefore simultaneously incorporated into the possible independent variable set in this study.

Subsequently, the MLSR analysis between each original water quality parameter versus the corresponding reflectance values of the OLI bands was undertaken separately. For the model development of each water quality parameter in each season, the aforementioned bands, as well as their ratios, were input into the model successively until no more improvements could be received from the new additional variables. Meanwhile, bands or band ratios which made undesirable contributions to the model, or showed lower correlations with the *in-situ* values of the water quality parameters than other variables having been included in the model, were excluded from the model (Figure 2). The number of selected predictor variables (either bands or band ratios) was limited to three in order to reduce the possibility of over-fitting and ensure the robustness (Hansen *et al*., 2015). Moreover, the coefficient of determination (R^2) and the mean squared error (MSE) were chosen as the two main evaluation criterions to select the optimal water quality models. R^2 values ought to be close to 1, and the MSE was required to be the minimum.

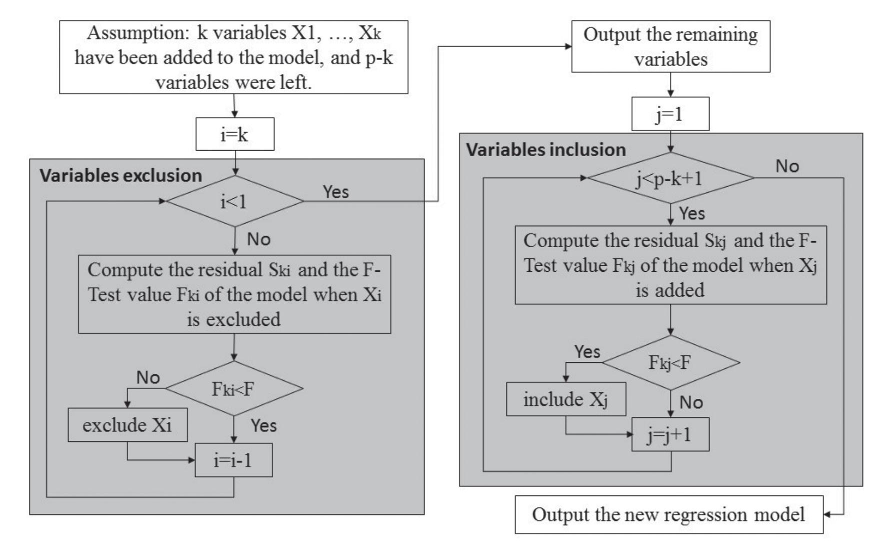

Figure 2. Variables exclusion/inclusion in MLSR method.

Results

Regression Models

Table 3 presents the best regression models for COD_{Mn}, BOD_5, TP, and TN in the two different seasons, with R^2 ranging from 0.51 to 0.81. Specifically, COD_{Mn} is found to be more closely related to OLI bands 5 and 6 (R^2 = 0.61 in the dry season and R^2 = 0.58 in the wet season). Meanwhile, BOD_5 is primarily related to OLI band 5 and shows a positive correlation with OLI band 7 in the wet season (R^2 = 0.81). Both TN and TP are most relevant to the visible and near-infrared regions (bands 2 to 5 and their combinations, with R^2 ranging from 0.51 to 0.62), with OLI band 6 being moderately correlated with TN in the wet season (R^2 = 0.64). Similar results were also reported by Chen and Quan (2012), who used TM bands 1 to 4 to estimate TP and TN concentrations in Tai Lake, with R^2 values of 0.63 and 0.24, respectively.

Table 3. The best regression models for predicting the water quality parameters in DJKR.

Season	Water quality parameter	Model	R^2	MSE	p-value
Dry season	COD_{Mn}	COD_{Mn}=67.06**B5*–31.37**B6* +1.42	0.61	2.487	<0.05
	BOD_5	BOD_5=26.83* *B5*–0.113	0.52	1.401	<0.05
	TP	TP=0.02**B3*/*B2*+1.24* *B5*–0.06	0.54	0.003	<0.05
	TN	TN=0.28* *B3*/ *B5*+21.07**B4*+0.74	0.62	1.146	<0.05
Wet season	COD_{Mn}	COD_{Mn}=–1.05* *B5*/ *B4*+51* *B6*+2.69	0.58	0.759	<0.05
	BOD_5	BOD_5=–7.54* *B5*+69.40**B7*+0.58	0.81	0.114	<0.05
	TP	TP=–0.07**B5*/*B3*+2.033**B5*	0.51	0.005	<0.05
	TN	TN=23.857**B6*+23.089**B4*–0.333	0.64	0.473	<0.05

**B2* to *B7* represent the normalized reflectance values of the corresponding OLI bands.

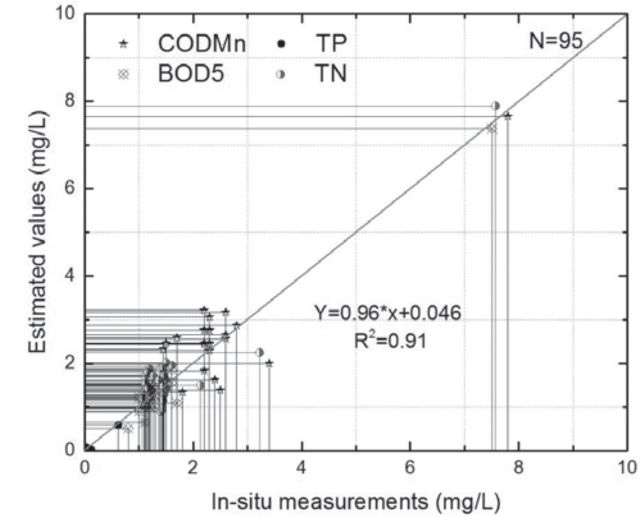

Figure 3. Relationships between the estimated values and the in-situ data measured on the acquisition dates of the 11 remaining images, with a 1:1 fit line. *N* represents the number of validation points.

The *in-situ* data measured on the acquisition dates of the 11 remaining images, which were not used for the model development, were chosen for further accuracy validation of the regression models. The best-fit models were applied to normalize the images and then obtain the estimated values of the corresponding water quality parameters. The relationships between the estimated values and the *in-situ* data are shown in Figure 3. These verification points are all evenly distributed close to the 1:1 line, and thus confirm the robustness of the developed models ($R^2 = 0.91$).

Water Quality Changes Over the Years

Compared with traditional water quality measurements, one of the great advantages of satellite images is that they can provide a synoptic view of water quality over a large-scale spatial area, which can be of considerable assistance to the investigation of the pre-existing or latent driving factors of water quality deterioration, as well as the appropriate decision-making for water conservation in DJKR. Accordingly, the validated water quality regression models were then applied to process Landsat images from May 2006 to May 2014, to obtain spatio-temporal water quality distribution maps of DJKR. The spatial distributions of these four water quality parameters inversed from the same Landsat image showed similar spatio-temporal patterns. Herein, we take the TN distribution maps for an example for detailed analyses.

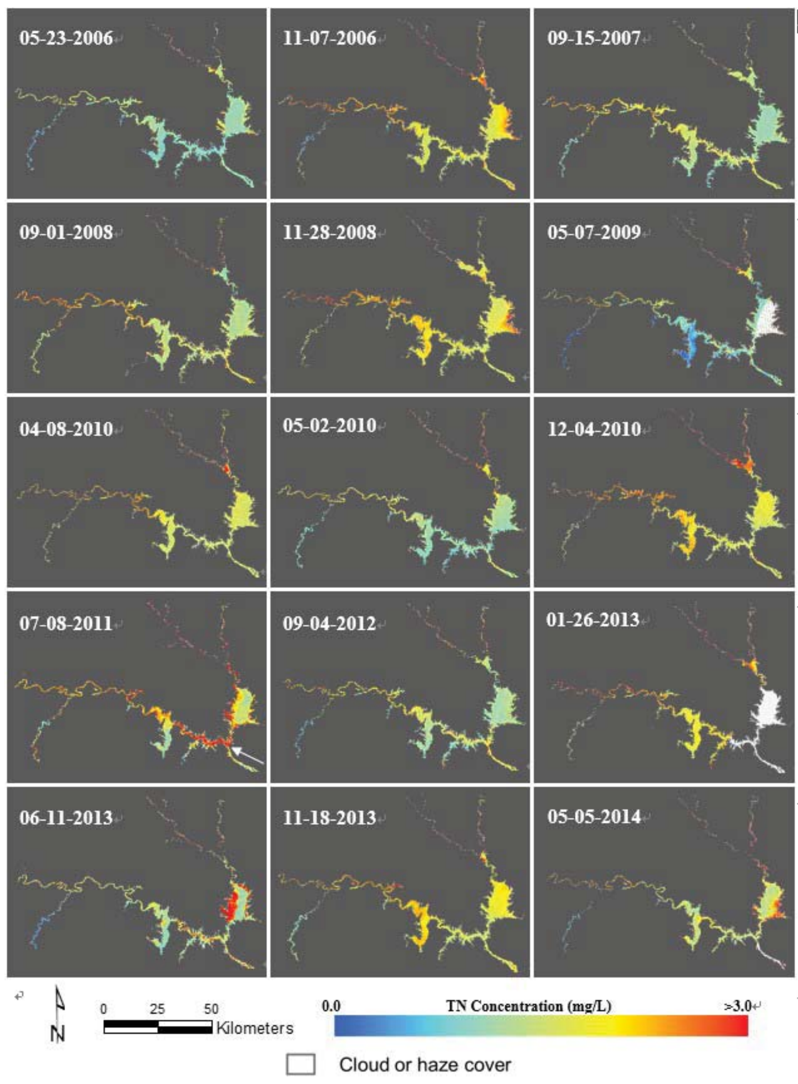

Figure 4. TN concentration distribution maps of DJKR and its tributaries from 2006 to 2014.

Figure 4 presents the distribution of the TN concentration in DJKR from 2006 to 2014, which differed significantly in the wet and dry seasons. For ease of quantitative comparison, we divided the area into three parts: the Dan reservoir, the Han reservoir, and the tributaries. In general, higher TN values were distributed primarily over the water/land interface area, the eastern Dan Reservoir, and where the tributaries enter the reservoir. On the basis of the results shown in Table 4, the values of TN concentration in the tributaries were much higher than in the reservoir in both seasons. It is also noteworthy that the TN concentration in Han Reservoir was lower in the southern area than in the north, yet, in Dan Reservoir, worse TN pollution was evident in the water/land interface area and the eastern region. Moreover, Dan Reservoir appeared to be more polluted than Han Reservoir in most cases (Table 4). Additionally, there were more homogeneous distributions and higher mean values of TN concentration in DJKR in the dry seasons than in the wet seasons, which suggests worse water quality in the reservoir in the dry seasons, coincident with Chen *et al.* (2015).

Figure 5 demonstrates the water quality variation from 2006 to 2013 in the DJKR area. In the period between May 2006 and May 2014, the values of all four water quality parameters showed deteriorating trends (+52.0 percent for TN, +29.2 percent for BOD_5, +16.1 percent for COD_{Mn}, and +133.3 percent for TP) in the DJKR area. Specifically, the mean concentration values fluctuated from May 2006 to May 2010, with TN (from 1.27 mg/L to 1.47 mg/L), BOD_5 (from 1.22 mg/L to 1.38 mg/L), and TP (from 0.03 mg/L to 0.04 mg/L) increasing and COD_{Mn} slightly decreasing from 2.67 mg/L to 2.65 mg/L. The water quality parameters reached a peak in July 2011, with the TN, BOD_5, COD_{Mn}, and TP concentration values reaching 2.2mg/L, 1.82mg/L, 3.4mg/L, and 0.08mg/L, respectively. Despite a significant decrease in 2012, the values of the four water quality parameters rebounded during 2012 to 2014. In addition, the values of TN

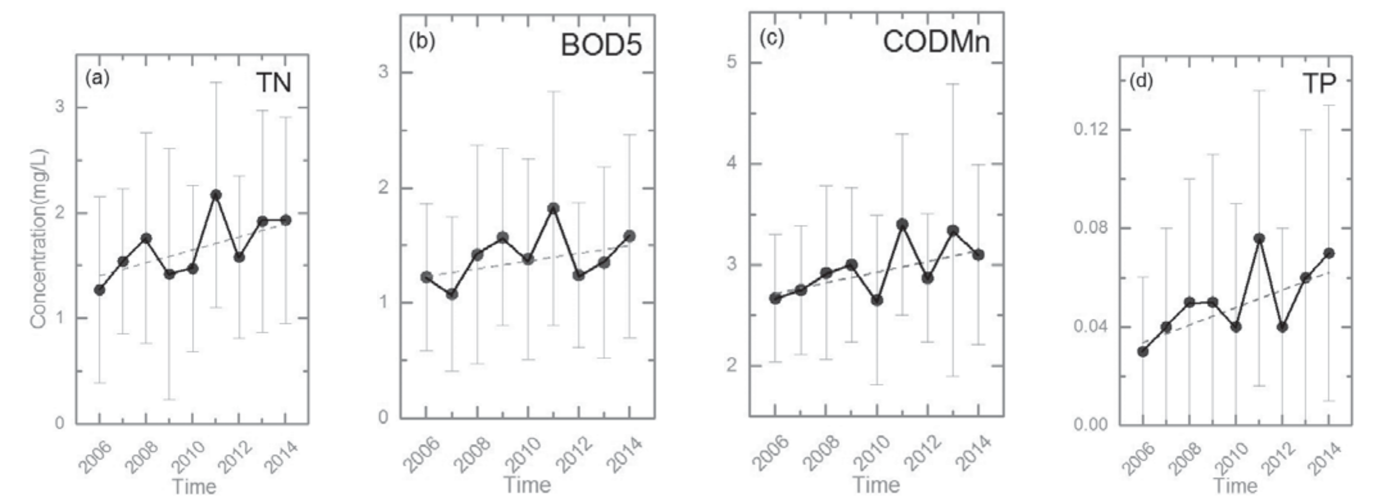

Figure 5. Mean concentration variability of (a) TN, (b) BOD$_5$, (c) COD$_{Mn}$, and (d) TP from 2006 to 2014. The horizontal lines in each plot represent the standard deviations of the values of the estimated water quality parameters.

Table 4. Comparison of the mean values of TN concentration in the Dan reservoir, Han reservoir, and the tributaries.

Season	Date	Dan Reservoir mean (mg/L)	Han Reservoir mean (mg/L)	Tributaries mean (mg/L)
Wet season	05/23/2006	1.27	1.16	1.45
	09/15/2007	1.22	1.57	1.83
	09/01/2008	1.47	1.59	2.30
	05/07/2009	1.64	0.65	1.46
	05/02/2010	1.37	1.27	1.87
	07/08/2011	1.93	1.84	2.29
	09/04/2012	1.33	1.55	1.92
	06/11/2013	2.18	1.41	1.92
	05/05/2014	1.91	1.64	2.46
Dry season	11/07/2006	1.97	1.88	2.39
	11/28/2008	1.93	2.10	2.08
	04/08/2010	1.74	1.75	2.20
	12/04/2010	1.81	2.13	2.36
	01/26/2013	/	1.93	2.36
	11/18/2013	1.39	1.68	2.09

concentration showed a substantial increase in both Dan Reservoir and Han Reservoir (+50.4 percent in Dan Reservoir and +41.4 percent in Han Reservoir) from 2006 to 2014 (Table 4). In general, the BOD$_5$, COD$_{Mn}$, and TP concentrations were stable at Grade I or II level, except for the tributaries and the terribly polluted seasons in 2011 and 2013. However, the mean TN values in the reservoir were constantly more than twice the limit values for Grade II waters, indicating severe TN pollution in DJKR over the past nine years.

Discussions and Analyses

Reflectance Issues

Atmospheric correction is one of the pivotal factors prior to the time-series satellite image analysis. However, in this study, both between-sensor differences and lack of information about the in-situ atmospheric conditions brought extra difficulties to the atmospheric correction. With the purpose of overcoming or rather reducing the influence of these two issues and preferably estimating the water quality parameters of DJKR, we applied one of the most accurate atmospheric correction method, i.e., FLAASH algorithm, which provides pre-defined *in-situ* atmospheric conditions, to obtain reliable surface reflectance values of the DJKR. At the same time, OLS method was used to normalize the **s**urface reflectance of the imagery time-series in order to ensure the between-sensor consistency.

Surface reflectance values before and after normalization of the between-sensor change were demonstrated in Figure 6. For ease of comparison, the reflectance values were stretched to 0-10000 to raise the gaps between the values. It is visible that the **s**urface reflectance values were more centralized and close to the 1:1 fit lines after normalization, particularly prominent in the dark areas. In other words, the surface reflectance values of the TM/ETM+ were much closer to the referenced OLI images when applied OLS correction. In the bright areas, normalization seemed to be less effective, especially in OLI bands 3 and 4. Due to the high reflectance, complex structure as well as mixed pixels of bright targets, estimating the land surface reflectance for bright surfaces using Landsat images has been a great challenge (Sun *et al.*, 2015). Given that only dark objects (i.e., water areas) were researched in this paper, the bias of normalization were considered to be negligible.

Causative Factors

The water quality parameters (COD$_{Mn}$, BOD$_5$, TP, and TN) retrieved by the multitemporal and multi-sensor Landsat images revealed a deteriorating water quality trend and showed a heterogeneous spatio-temporal distribution in DJKR during the observation period. Both natural and human factors were analyzed to investigate the causative factors of the water quality distribution and the driving forces of the water pollution.

Natural Factors

The LULC maps of the DJKR catchment area presented in Figure 7 showed that the land-use types along the tributaries were mainly farmland and grassland, which were confronted with high soil erosion risk as well as heavy eco-environmental vulnerability (Li *et al.*, 2009; Wang *et al.*, 2013), especially along the Dan River. Farmland, grassland, and shrub land accounted for more than 65 percent (69.1 percent in 2005 and 68.07 percent in 2015) of the total area (Table 5). A large area of forest (116 km^2) was transformed into grassland and shrub land (Figure 7), while the area of building land increased by 177.89 km^2 in 2015 compared with that in 2005. Thus, the ability for soil and water conservation was reduced. Additionally, the high mountains and steep slopes around the reservoir also increase the soil erosion risk in this area (Wang *et al.*, 2003; Wang *et al.*, 2013). In the meantime, continuous and heavy rainfall in the wet seasons greatly aggravates

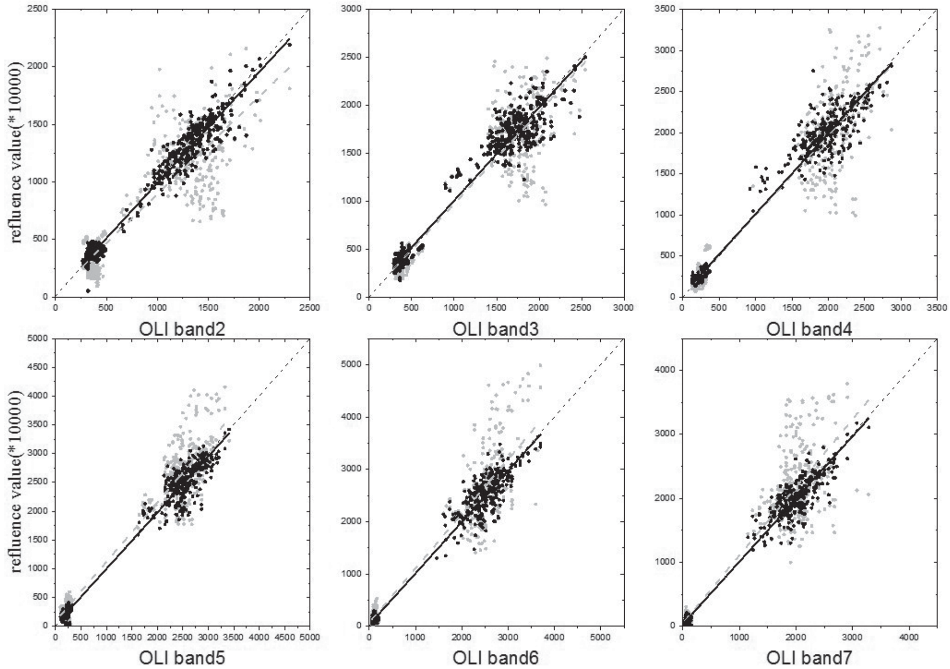

Figure 6. Surface reflectance values before (grey points) and after (black points) normalization of the between-sensor change (totally 1,332 points). The grey dash lines and black solid lines represent the fitted lines of the reflectance values before and after normalization, respectively.

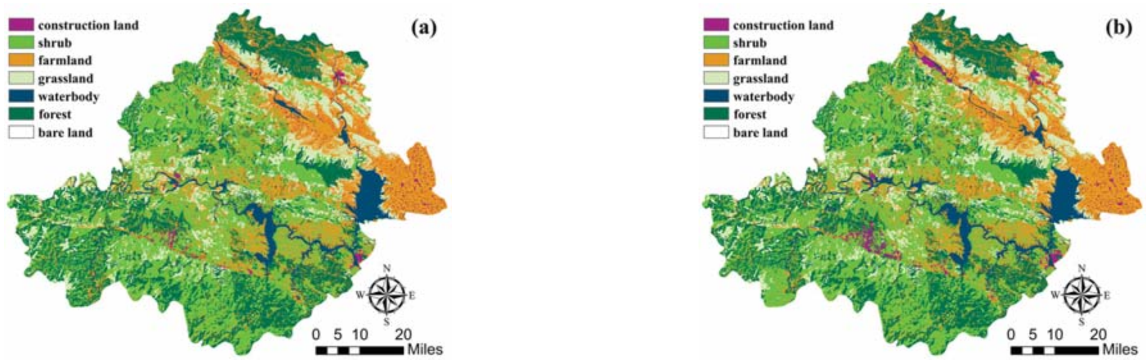

Figure 7. The LULC maps of the DJKR catchment in (a) 2005, (b) 2010, and (c) 2015.

soil erosion and then causes soil material sedimentation in DJKR and its tributaries. As a result, the high soil erosion risk in this area ultimately leads to the water pollution in DJKR, especially in the water/land interface area and where the tributaries enter the reservoir. The severe water pollution in July 2001 and June 2013 was mostly due to the stony desertification resulting from vegetation reduction and the heavy rainfall near the dates of the image acquisition (Hubei Daily, 2013; China Meteorological Administration, 2015). Moreover, the heavy rainfall and the torrents in the wet seasons disperse the contaminants in the reservoir and lead to inhomogeneity of the water quality distribution, which can partly explain the differences between the wet and dry seasons.

Table 5. Comparison of the area of each land-use type in the DJKR catchment area between 2005 and 2015.

	2005		2015	
Land-use type	Area (km²)	Percentage (%)	Area (km²)	Percentage (%)
Farmland	2606.71	23.93	2502.50	22.97
Forest	2646.78	24.30	2530.83	23.24
Shrub land	3532.59	32.43	3551.30	32.61
Grassland	1387.56	12.74	1360.15	12.49
Bare land	20.66	0.19	19.16	0.18
Built-up land	133.07	1.22	310.96	2.86
Water body	565.45	5.19	616.51	5.65

Human Activities

As presented in Figure 1, four state-level poverty-stricken counties and one prefecture-level city are located along the tributaries. The large population (more than 4 million in 2014) inevitably leads to intensive agricultural and industrial activities, and thus causes both point-source and non-point-source pollution.

Intensive agricultural activities over large areas of farmland will generally result in the use of massive amounts of nitrogenous and phosphorus fertilizers. Considering the fact that the utilization rates of the fertilizers were found to be less than 40 percent, redundant nitrogen and phosphorus in the soil will ultimately enter into the reservoir and tributaries through runoff as well as underground water (Liu *et al.*, 2014). Figure 8a indicates a significant relationship between the annual amount of fertilizer applied in the study area and the mean concentration of TN ($R^2 = 0.36$, $p < 0.1$). In other words, the fertilizer use can explain about 36 percent of the severe nitrogen pollution in the DJKR area. It is also apparent that the regions with larger TN values are generally adjacent to larger areas of farmland, especially around Dan Reservoir, as confirmed in Figure 4. However, the correlation between the amount of fertilizer applied and the values of the TP concentration are relatively weak ($R^2 = 0.19$, $p > 0.1$) (Figure 8b). Indeed, municipal effluents, livestock waste, and other latent causative factors can also lead to nitrogen or phosphorus pollution, hence, additional data is required for more comprehensive investigation.

BOD_5 and COD_{Mn} mainly stem from activities such as industrial effluent and domestic sewage (Chen *et al.*, 2015; Zhu *et al.*, 2008). The prefecture-level city, Shiyan, located by the Han River, is well known for its automobile industry. In addition, Xichuan is recognized as the largest producer of vanadium ore in Henan province. Waste water was mainly discharged into local tributaries, which could explain the severe BOD_5 and COD_{Mn} pollution in the tributaries, and eventually flowed into the reservoir. Figure 9 shows a weak correlation between the annual sewage discharge and the mean BOD_5 concentration in the DJKR area from 2006 to 2014 ($R^2 = 0.25$, $p > 0.1$). However, the increasing trend of the annual sewage discharge closely corresponds to the trend of BOD_5 over the study period, which demonstrate that the sewage discharge can be considered as a driving factor of the increasing BOD_5 concentrations in the study area, and COD_{Mn} can be explained likewise. Additionally, it is noteworthy that the tributaries played dominant roles in the transportation of BOD_5 and COD_{Mn} to DJKR.

Likewise, the construction of the Danjiangkou Dam may have impacted the water quality distribution in the reservoir. The dam was elevated from 162.0 m to 176.6 m for the SNWT Project from 2005 to 2010. However, the increase of the water level led to increased water retention times and imposed restrictions on the discharge of contaminants (Chen *et al.*, 2016). The water quality distribution maps for the wet season of July 2011 present a clear dividing line at the dam (Figure 4). In addition, the upland water greatly decreases in the dry seasons, and the outflow of water at the dam is generally reduced by human intervention to stabilize the water storage in DJKR, which further increases the time of contaminant retention. The more severe TN pollution of DJKR in the dry seasons between 2006 and 2014, as shown in Table 4, could be attributable to this reason. Therefore, the obstruction of the dam augments the sedimentation of soil nutrients and aggravates the deterioration of water quality in the reservoir.

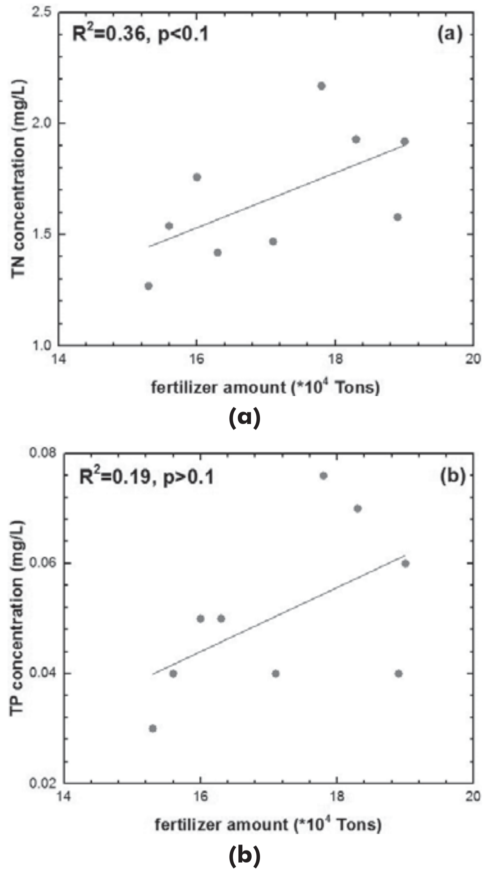

Figure 8. Relationships between the annual fertilizer amount and the mean concentration of (a) TN, and (b) TP retrieved by regression models.

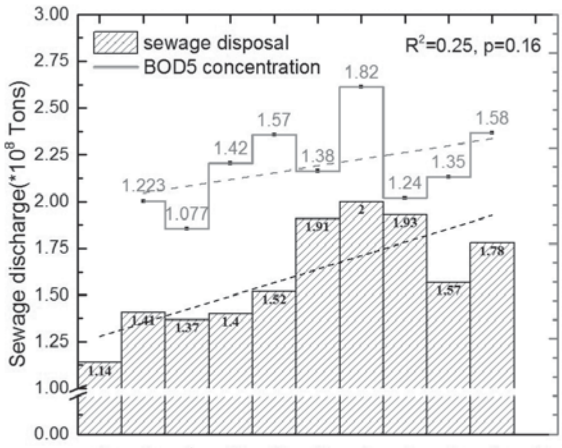

Figure 9. The annual sewage discharge in the DJKR area and the mean BOD_5 concentration retrieved in this study during the observation period. The blue and gray dashed lines are the trend lines of the BOD_5 concentration and sewage discharge variations, respectively.

Conclusions

In this study, we used multi-temporal and multi-sensor Landsat images from 2006 to 2014 to obtain long-term observations of the distribution and variation of COD_{Mn}, BOD_5, TP, and TN in DJKR. The water quality distribution maps retrieved from the time series of Landsat images presented considerable heterogeneity of water quality distribution and also revealed severe TN pollution in the DJKR area during the observation period. The heavily polluted regions were distributed primarily in the water/land interface area, the eastern Dan Reservoir, and where the tributaries enter the reservoir. Additionally, DJKR showed a more homogeneous water quality distribution in the dry seasons, which was likely due to the relatively low stream flow in the tributaries and reservoir in the dry seasons, as well as the construction of the Danjiangkou Dam. Furthermore, the concentration of the water quality parameters in the tributaries was much higher than that in the reservoir in both seasons, which indicates the more severe pollution in the tributaries. The tributaries have become a dominant conveyor of contaminants, and thus pose a threat to the water quality in DJKR.

The long-term water quality variation showed a significant deteriorating trend, which appeared to be driven by both natural and human factors. For instance, the increase of the BOD_5 and COD_{Mn} concentrations could be linked to sewage discharge. The soil erosion and the massive use of fertilizer could partly explain the severe TN pollution in this area. Even though the government has taken steps to improve the water quality in DJKR in recent years, e.g., through conversion of farmland to forest and reducing the number of factories, this study indicated that more effective measures are urgently needed. The information provided in this study should not merely raise public alarm, but should also provide an essential reference for local government to make appropriate and comprehensive policies for water quality improvement in DJKR, and ensure the implementation of the South-North Water Transfer (SNWT) Project.

Acknowledgments

The work presented in this paper was supported in part by China Science Fund for Excellent Young Scholars under Grant 41522110, in part by the National Key Research and Development Program of China under Grant 2016YFB0501403, and in part by the Foundation for the Author of National Excellent Doctoral Dissertation of PR China (FANEDD) under Grant 201348. The authors would like to thank the anonymous reviewers for their insightful and constructive comments, which significantly improved the quality of this paper.

References

Bonansea, M., M.C. Rodriguez, L. Pinotti, and S. Ferrero, 2015. Using multi-temporal Landsat imagery and linear mixed models for assessing water quality parameters in Río Tercero reservoir (Argentina), *Remote Sensing Of Environment*, 158:28–41.

Brezonik, P., K.D. Menken, and M. Bauer, 2005. Landsat-based remote sensing of lake water quality characteristics, including chlorophyll and Colored Dissolved Organic Matter (CDOM), *Lake and Reservoir Management*, 21:373–382.

Çamdevýren, H., N. Demýr, A. Kanik, and S. Keskýn, 2005. Use of principal component scores in multiple linear regression models for prediction of Chlorophyll-a in reservoirs, *Ecological Modelling*, 181:581–589.

Canty, M.J., A.A. Nielsen, and M. Schmidt, 2004. Automatic radiometric normalization of multitemporal satellite imagery, *Remote Sensing Of Environment*, 91:441–451.

Chen, J., and W. Quan, 2012. Using Landsat/TM imagery to estimate nitrogen and phosphorus concentration in Taihu Lake, China, *IEEE Journal of Selected Topics in Applied Earth Observations and Remote Sensing*, 5:273–280.

Chen, L., Z. Yang, and H. Liu, 2016. Assessing the eutrophication risk of the Danjiangkou Reservoir based on the EFDC model, *Ecological Engineering*, 96:117–127.

Chen, P., L. Li, and H. Zhang, 2015. Spatio-temporal variations and source apportionment of water pollution in Danjiangkou Reservoir Basin, Central China, *Water*, 7:2591–2611

China Meteorological Administration, 2015. Monthly precipitation dataset of China (1981-2015), URL: *http://data.cma.cn/* (last date accessed: 31 July 2017).

Cooley, T., G.P. Anderson, G.W. Felde, M.L. Hoke, A.J. Ratkowski, J.H. Chetwynd, J.A. Gardner, S.M. Adler-Golden, M.W. Matthew, A. Berk, L.S. Bernstein, P.K. Acharya, D. Miller, and P. Lewis, 2002. FLAASH, a MODTRAN4-based atmospheric correction algorithm, its application and validation, *Proceedings of the IEEE International Geoscience and Remote Sensing Symposium*, 2002. *IGARSS '02. 2002*, 1413:1414-1418.

Du, Y., P.M. Teillet, and J, Cihlar, 2002. Radiometric normalization of multitemporal high-resolution satellite images with quality control for land cover change detection, *Remote Sensing Of Environment*, 82:123–134.

Feng, L., X. Han, C. Hu, and X. Chen, 2016. Four decades of wetland changes of the largest freshwater lake in China: Possible linkage to the Three Gorges Dam?, *Remote Sensing of Environment*, 176:43–55.

Flood, N.,2014. Continuity of reflectance data between Landsat-7 ETM+ and Landsat-8 OLI, for both top-of-atmosphere and surface reflectance: A Study in the Australian landscape, *Remote Sensing*, 6:7952–7970.

Gu, S., X. Cheng, Z. Shen, and Q. Zhang, 2008. Watershed characteristics of the upper reaches of the Hanjiang River basin, *Resources and Environment in the Yangtze Basin*.

Guan, X., J. Li, and W.G. Booty, 2011. Monitoring Lake Simcoe water clarity using Landsat-5 TM images, *Water Resources Management*, 25:2015–2033.

Han, X., X. Chen, and L. Feng, 2015. Four decades of winter wetland changes in Poyang Lake based on Landsat observations between 1973 and 2013, *Remote Sensing of Environment*, 156:426–437.

Hansen, C.H., G.P. Williams, Z. Adjei, A., Barlow, E.J. Nelson, and A.W. Miller, 2015. Reservoir water quality monitoring using remote sensing with seasonal models: Case study of five central-Utah reservoirs, *Lake and Reservoir Management*, 31:225–240.

Hubei Daily, 2013. The creazy stony desertification in Henan Province, URL: *http://newpaper.dahe.cn/hnsb/html/2013-06/29/content_916549.htm* (last date accessed: 31 July 2017).

Kloiber, S.M., P.L. Brezonik, and M.E. Bauer, 2002. Application of Landsat imagery to regional-scale assessments of lake clarity, *Water Research*, 36:4330–4340.

Lamaro, A.A., A. Mariñelarena, S.E. Torrusio, and S.E. Sala, 2013. Water surface temperature estimation from Landsat 7 ETM+ thermal infrared data using the generalized single-channel method: Case study of Embalse del Río Tercero (Córdoba, Argentina), *Advances In Space Research*, 51:492–500.

Lathrop, R.G., 1992. Landsat Thematic Mapper monitoring of turbid inland water quality, *Photogrammetric Engineering & Remote Sensing*, ASPRS, 58:465–470.

Li, L., Z.-H. Shi, W. Yin, D. Zhu, S.L. Ng, C.-F. Cai, and A.L. Lei, 2009. A fuzzy analytic hierarchy process (FAHP) approach to eco-environmental vulnerability assessment for the Danjiangkou Reservoir area, China, *Ecological Modelling*, 220:3439–3447.

Li, S.-Y., and Q.-F Zhang, 2005. Analysis on solving issues of water use in the northern China through South North Water Transfer Project, *Yellow River*, 27:28–29.

Liu, R., Y. Kang, C. Zhang, L. Pei, S. Wan, S. Jiang, S. Liu, S., Z. Ren, and Y. Yang, 2014. Chemical fertilizer pollution control using drip fertigation for conservation of water quality in Danjiangkou Reservoir, *Nutrient Cycling In Agroecosystems*, 98:295–307.

Lo, C.P., and X. Yang, 2000, Relative radiometric normalization performance for change detection from multi-date satellite images, *Photogrammetric Engineering & Remote Sensing*, 66:967–980.

Lobo, F.L., M.P. Costa, and E.M. Novo, 2015. Time-series analysis of Landsat-MSS/TM/OLI images over Amazonian waters impacted by gold mining activities, *Remote Sensing of Environment*, 157:170–184.

Loveland, T.R., and J.L. Dwyer, 2012. Landsat: Building a strong future, *Remote Sensing of Environment*, 122:22–29.

McCullough, I.M., C,S, Loftin, and S.A. Sader, 2012. Combining lake and watershed characteristics with Landsat TM data for remote estimation of regional lake clarity, *Remote Sensing of Environment*, 123:109–115.

Oki, K., 2010. Why is the ratio of reflectivity effective for chlorophyll estimation in the lake water?, *Remote Sensing*, 2:1722–1730.

Pastorguzman, J., P. Atkinson, J. Dash, and R. Riojanieto, 2015.. Spatotemporal variation in mangrove chlorophyll concentration using Landsat 8, *Remote Sensing*, 7:14530–14558.

Ritchie, J.C., 2003. Remote sensing techniques to assess water quality, *Photogrammetric Engineering & Remote Sensing*, 69:695–704.

Selst, M.V.,and P. Jolicoeur, 1994. A solution to the effect of sample size on outlier elimination, *The Quarterly Journal of Experimental Psychology*, 47:631–650.

Song, C., C.E. Woodcock, K.C. Seto, M.P. Lenney, and S.A. Macomber, 2001. Classification and change detection using Landsat TM Data, When and how to correct atmospheric effects?, *Remote Sensing Of Environment*, 75:230–244.

Sriwongsitanon, N., K. Surakit, and S. Thianpopirug, 2011. Influence of atmospheric correction and number of sampling points on the accuracy of water clarity assessment using remote sensing application, *Journal Of Hydrology*, 401:203–220.

Sun, L., J. Wei, M. Bilal, X. Tian, C. Jia, Y. Guo, and X. Mi, 2015. Aerosol optical depth retrieval over bright areas using Landsat 8 OLI images, *Remote Sensing*, 8:23.

Tebbs, E.J., J.J. Remedios, and D.M. Harper, 2013. Remote sensing of chlorophyll-a as a measure of cyanobacterial biomass in Lake Bogoria, A hypertrophic, saline-alkaline, flamingo lake, using Landsat ETM+, *Remote Sensing Of Environment*, 135:92–106.

USGS, 2014. USGS Global Visualization Viewer URL: *http://glovis.usgs.gov/* (last date accessed: 31 July 2017).

Wang, G., G. Gertner, S. Fang, and A.B. Anderson, 2003. Mapping multiple variables for predicting soil loss by geostatistical methods with TM Images and a slope map, *Photogrammetric Engineering & Remote Sensing*, 69:889–898.

Wang, L., J. Huang, Y. Du, Y. Hu, Y., and P. Han, 2013. Dynamic assessment of soil erosion risk using Landsat TM and HJ satellite data in Danjiangkou Reservoir area, China. *Remote Sensing*, 5:3826–3848.

Xin, X.-K., K.-F Li, B. Finlayson, and W. Yin, 2015. Evaluation, prediction, and protection of water quality in Danjiangkou Reservoir, China, *Water Science and Engineering*, 8:30–39.

Xu, H., 2006. Modification of normalised difference water index (NDWI) to enhance open water features in remotely sensed imagery, *International Journal of Remote Sensing*, 27:3025–3033.

Zhang, Q., Z. Xu, Z. Shen, S. Li, and S. Wang, 2009. The Han River watershed management initiative for the South-to-North Water Transfer project (Middle Route) of China, *Environmental Monitoring and Assessment*, 148:369–377.

Zhu, Y.P., H.P. Zhang, L. Chen, and J.F. Zhao, 2008. Influence of the South-North Water Diversion Project and the mitigation projects on the water quality of Han River, *Science of the Total Environment*, 406:57–68.